Partial Deconvolution With Inaccurate Blur Kernel

Dongwei Ren, Wangmeng Zuo, David Zhang, Jun Xu, and Lei Zhang

***Abstract*— Most non-blind deconvolution methods are developed under the error-free kernel assumption, and are not robust to inaccurate blur kernel. Unfortunately, despite the great progress in blind deconvolution, estimation error remains inevitable during blur kernel estimation. Consequently, severe artifacts such as ringing effects and distortions are likely to be introduced in the non-blind deconvolution stage. In this paper, we tackle this issue by suggesting: 1) a partial map in the Fourier domain for modeling kernel estimation error, and 2) a partial deconvolution model for robust deblurring with inaccurate blur kernel. The partial map is constructed by detecting the reliable Fourier entries of estimated blur kernel. And partial deconvolution is applied to wavelet-based and learning-based models to suppress the adverse effect of kernel estimation error. Furthermore, an E-M algorithm is developed for estimating the partial map and recovering the latent sharp image alternatively. Experimental results show that our partial deconvolution model is effective in relieving artifacts caused by inaccurate blur kernel, and can achieve favorable deblurring quality on synthetic and real blurry images.**

***Index Terms*— Image deblurring, blind deconvolution, blur kernel estimation, E-M algorithm.**

I. Introduction

IMAGE deblurring that aims to recover clean image from its blurry observation is a fundamental problem in image processing and low level vision. By assuming the blur is spatially uniform, the blurry image $\mathbf{y}$ can be formulated as the convolution of blur kernel $\mathbf{k}$ with a sharp image $\mathbf{x}$,

$$\mathbf{y} = \mathbf{k} \otimes \mathbf{x} + \mathbf{n}, \tag{1}$$

where $\otimes$ denotes 2D convolution operation, and $\mathbf{n}$ is additive white Gaussian noise (AWGN). Moreover, with the uniform blur assumption, image deblurring can be formulated into a deconvolution problem [1].

Manuscript received April 1, 2017; revised August 25, 2017; accepted October 10, 2017. Date of publication October 18, 2017; date of current version November 9, 2017. This work was supported in part by the National Key R&D Program of China under Grant 2017YFC0113000, in part by the NSFC under Grant 61671182 and Grant 61471146 and in part by the Hong Kong RGC General Research Fund under Grant PolyU 5313/12E. The associate editor coordinating the review of this manuscript and approving it for publication was Prof. Ling Shao. *(Corresponding author: Wangmeng Zuo.)*

D. Ren and D. Zhang are with the School of Computer Science and Technology, Harbin Institute of Technology, Harbin 150001, China, and also with the Department of Computing, The Hong Kong Polytechnic University, Hong Kong (e-mail: rendongweihit@gmail.com; csdzhang@comp.polyu.edu.hk).

W. Zuo is with the School of Computer Science and Technology, Harbin Institute of Technology, Harbin 150001, China (e-mail: cswmzuo@gmail.com).

J. Xu and L. Zhang are with the Department of Computing, The Hong Kong Polytechnic University, Hong Kong (e-mail: csjunxu@comp.polyu.edu.hk; cslzhang@comp.polyu.edu.hk).

Color versions of one or more of the figures in this paper are available online at http://ieeexplore.ieee.org.

Digital Object Identifier 10.1109/TIP.2017.2764261

Blind deconvolution is a more challenging deblurring problem, in which both the blur kernel and the sharp image are unknown. A typical blind deconvolution method generally involves two stages: (i) blur kernel estimation from the blurry observation and (ii) non-blind deconvolution based on the estimated blur kernel. By far, various methods, including Variational Bayes (VB) [2], Maximum a Posterior (MAP) [1] and their extensions [3]–[13], have been proposed for blur kernel estimation. With the estimated blur kernel, the existing non-blind deconvolution approaches, e.g., total variation [14], hyper-Laplacian [15], EPLL [16], NCSR [17], and CNN-based methods [18], [19], can then be employed to recover the latent sharp image.

Despite the great progress in blur kernel estimation, the kernel error remains inevitable to be introduced. However, typical non-blind deconvolution methods are developed under the error-free kernel assumption [16], [20], [21], and are not robust to inaccurate blur kernel. Consequently, artifacts such as ringing effects and distortions are likely to be produced in the non-blind deconvolution stage.

Several methods have been proposed to design specific image priors to suppress the adverse effect caused by kernel estimation error. Given the estimated blur kernel $\mathbf{k}$, the sharp image $\mathbf{x}$ can be recovered in the MAP framework,

$$\begin{aligned}\mathbf{x} &= \arg\max_{\mathbf{x}} \log \Pr(\mathbf{x}|\mathbf{y}, \mathbf{k}) \\ &= \arg\max_{\mathbf{x}} \log \Pr(\mathbf{y}|\mathbf{k}, \mathbf{x}) + \log \Pr(\mathbf{x}).\end{aligned} \tag{2}$$

With error-free kernel assumption, the conditional probability distribution $\Pr(\mathbf{y}|\mathbf{k}, \mathbf{x})$ is commonly specified as Gaussian based on the noise $\mathbf{n}$. As for the regularization term $\log \Pr(\mathbf{x})$, extensive works [14]–[17], [22] have been proposed for modeling natural image priors. Instead of natural image priors, the structure consistency between the blurry and recovered sharp images is enforced in [23] and [24] for relieving ringing artifacts. In [25], bilateral regularization is iteratively imposed on the intermediate image to restore sharp edges. In [26], cross-channel priors were designed to reduce ringing effect.

However, the specifically designed image priors may fail in addressing complex artifacts. Denote by $\mathbf{k}^{gt}$ the groundtruth blur kernel. Even small blur kernel estimation error $\Delta\mathbf{k} = \mathbf{k}^{gt} - \mathbf{k}$ can produce severe artifacts such as ringing and distortions [24]. Thus, besides specific image priors, we should also take into account the characteristics of kernel estimation error for better suppressing the artifacts. To the best of our knowledge, there is only one attempt [27] to model kernel estimation error with an implicit strategy. Ji and Wang [27] introduce an auxiliary variable $\mathbf{r} = \Delta\mathbf{k} \otimes \mathbf{x}$ and then impose sparsity regularization on it. Although this method is effective

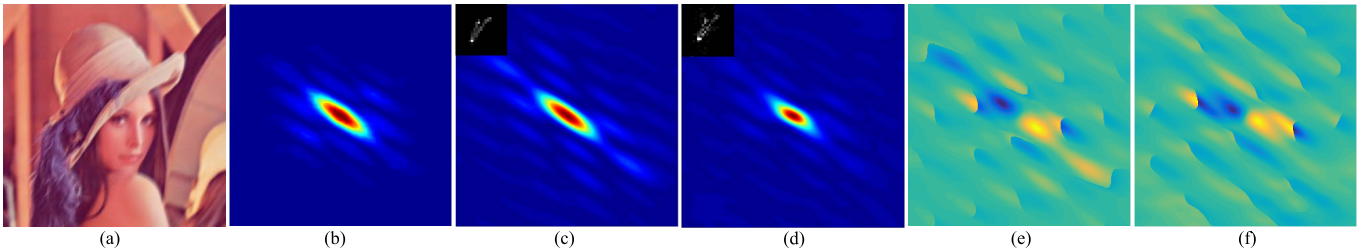

Fig. 1. An example of Fourier spectrum. The FS of groundtruth blur kernel is much different with that of estimated blur kernel, but is more similar with the reference FS by spectral method [28]. Moreover, the estimation error in phase is closely related with that in FS. Thus, we suggest to model blur kernel estimation error in Fourier domain by employing the reference FS to localize the reliable Fourier entries. (a) Blurry image. (b) Reference FS. (c) Groundtruth kernel and its FS. (d) Estimated kernel and its FS. (e) Weighted phase of groundtruth kernel. (f) Weighted phase of estimated kernel.

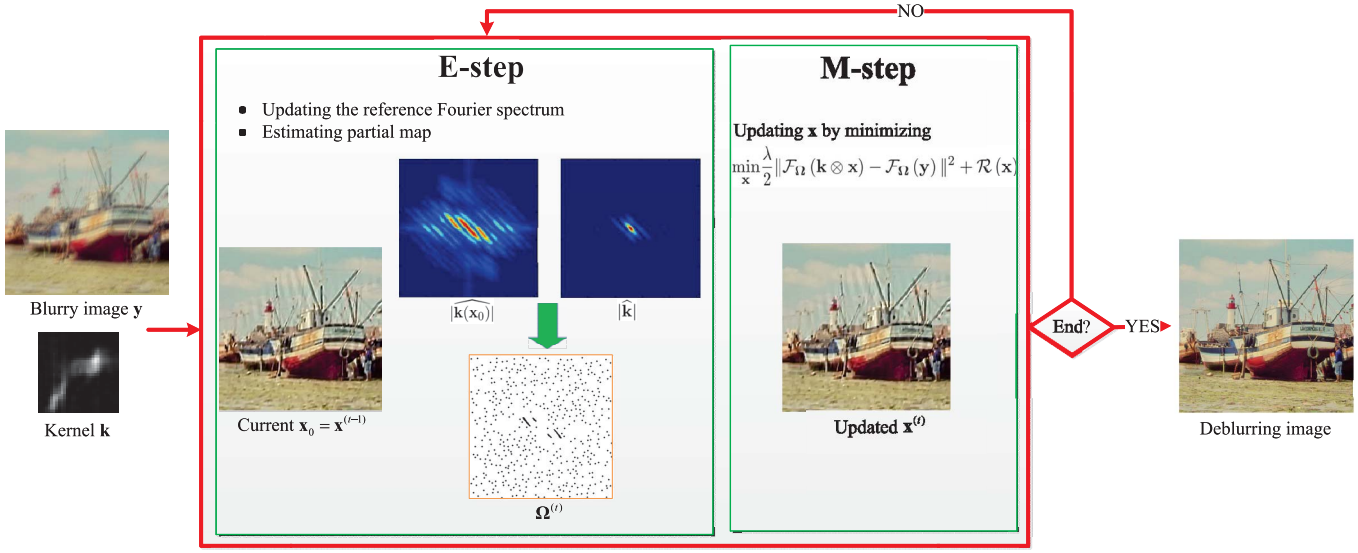

Fig. 2. Illustration of partial deconvolution under the E-M framework, where the E-step estimates the partial map and the M-step updates clean image.

in suppressing the artifacts, it also tends to over-smooth the texture details in the recovered images.

A. Motivation and Contributions

In this work, we aim to explicitly model kernel estimation error $\Delta\mathbf{k}$. Due to the groundtruth blur kernel is unknown, $\Delta\mathbf{k}$ is dependent with both the blurry image and kernel estimation algorithm, making it difficult to model $\Delta\mathbf{k}$ in spatial domain. Instead, we suggest to model $\Delta\mathbf{k}$ in Fourier domain. Fig. 2(c)(d) shows the Fourier spectrum (FS) of the groundtruth and estimated [29] blur kernels. And Fig. 2(e)(f) shows the magnitude-weighted phase information of the groundtruth and estimated [29] blur kernels. It is interesting to see that, the estimation error in phase is closely related with that in FS. Given one entry, when the FS of the estimated kernel is dissimilar to that of the groundtruth, it is very likely that the corresponding spectrum-weighted phase of the estimated kernel is also dissimilar to that of the groundtruth. Thus, one may model kernel estimation error in Fourier domain, but groundtruth FS is still required for reference. Fortunately, as shown in Fig. 2(b), the FS of blur kernel can be robustly estimated by several spectral methods [28], [30], and serves as a reasonable reference FS to localize the reliable Fourier entries for modeling kernel estimation error.

Motivated by this observation, we in this paper propose a partial deconvolution model to explicitly model kernel estimation error in Fourier domain. Given the reference FS, by comparing it with the FS of estimated blur kernel, a binary partial map $\mathbf{\Omega}$ can be constituted to indicate the reliability of Fourier entries of blur kernel. During deconvolution, only the reliable components ($\mathbf{\Omega}_i = 1$) within the partial map are used, whereas excluding the unreliable ones ($\mathbf{\Omega}_i = 0$), suppressing the adverse effect of kernel estimation error. Specifically, when the blur kernel is accurate, *i.e.*, each entry in $\mathbf{\Omega}$ is 1, the partial deconvolution model is exactly equivalent to the conventional deconvolution model in Fourier domain.

As for the joint estimation of the partial map and latent clean image, we develop an E-M framework, where the E-step is adopted to find the expectation of the partial map, and the M step performs partial deconvolution given partial map to recover clean image. The overall framework is illustrated as Fig. 2, which iteratively performs the following two steps: (i) In the E-step, given the current estimate of clean image $\mathbf{x}_0$, the reference FS can be estimated from the blurry image $\mathbf{y}$. The partial map $\mathbf{\Omega}$ is then updated by comparing with the FS of inaccurate blur kernel. (ii) In the M-step, given the partial map $\mathbf{\Omega}$, clean image $\mathbf{x}$ can be updated by solving the partial deconvolution. Specifically, by incorporating with wavelet-based [31] and learning-based [32] deconvolution models, two robust partial deconvolution methods are developed in this paper to recover clean image.

Moreover, we provide a variant of partial deconvolution model, in which zero points in FS of blur kernel are included into $\mathbf{\Omega}$. In [33], the authors suggest that zero points in FS

take charge of ringing effects, and propose a post-processing technique to detect and remove ringing effect with accordance to each zero point. Thus, the computational complexity in [33] is proportional to the number of zero points. But in our work, the partial deconvolution model and its variant share the same computational cost, and the de-ringing capability is naturally integrated into the deconvolution stage.

We summarize our contributions as follows:

- A novel partial deconvolution model is proposed for robust deblurring to inaccurate blur kernel by explicitly modeling kernel estimation error in Fourier domain.
- By incorporating partial deconvolution model with wavelet-based and learning-based methods, two robust deconvolution methods are developed for inaccurate blur kernel.
- Instead of post-processing, de-ringing with zero points in FS can be naturally integrated into the partial deconvolution model without the sacrifice of computational cost.

Experiments on synthetic datasets and real blurry images validate the effectiveness of the partial deconvolution model. The proposed methods achieve better quantitative metrics and visual quality than the state-of-the-art methods on the synthetic datasets. The results on real blurry images further indicate that the proposed methods can relieve not only ringing effects but also other artifacts like color distortions, leading to more visually plausible restoration quality.

B. Organization and Notations

The remainder of this paper is organized as follows. Section III proposes the partial deconvolution model along with the E-M framework for jointly estimating the partial map and clean image. Section IV applies the partial deconvolution into wavelet-based and learning-based methods for robust deblurring. Section V reports the experimental results, and Section VI concludes this paper.

In this paper, we use a bold lowercase, e.g., $\mathbf{x}$, to represent a 2D image and its vectorization. For a blur kernel or filter, e.g., $\mathbf{k}$, its uppercase $\mathbf{K}$ represent the corresponding sparse transform matrix. For the Fourier transform, $\mathcal{F}$ is the 2D Fourier transform, and $\mathbf{F}$ is the corresponding Fourier transform matrix. So for an image $\mathbf{x}$, its Fourier transform can be equivalently performed as $\hat{\mathbf{x}} = \mathcal{F}(\mathbf{x})$ or $\hat{\mathbf{x}} = \mathbf{F}\mathbf{x}$, where the former $\mathbf{x}$ is a 2D image, while the latter one is vectorized.

II. Related Work

In this section, we first review deconvolution methods based on natural image priors with error-free kernel assumption, and then present specifically designed priors and models for robust deconvolution with inaccurate blur kernel.

A. Deconvolution Based on Natural Image Prior

According to Eqn. (2), the non-blind deconvolution model can be equivalently reformulated as,

$$\mathbf{x} = \arg\min_{\mathbf{x}} \frac{\lambda}{2}\|\mathbf{k} \otimes \mathbf{x} - \mathbf{y}\| + \mathcal{R}(\mathbf{x}), \tag{3}$$

where $\mathcal{R}(\mathbf{x}) = -\log \Pr(\mathbf{x})$ is the regularization term associated with image prior, and λ is a positive trade-off parameter. With error-free kernel estimation, the fidelity term is usually specified as ℓ_2-norm corresponding to the AWGN $\mathbf{n}$. As for the regularization term, the key issue is to better describe priors of natural images. First, gradient-based models, such as total variation [34] and hyper Laplacian [15], are studied to model the distribution of image gradients, and have been widely applied due to its simplicity and efficiency. Then, patch-based [16] and non-local similarity [35], [36] models are developed to characterize more complex and internal dependence among image patches. Besides, by employing sparsity in wavelet domain [31], wavelet frame-based models are designed in both analysis and synthesis forms. Recently, under the discriminative learning framework, regression tree fields (RTF) [37] and cascaded shrinkage field (CSF) [22] are proposed to learn natural image priors with high computational efficiency. Besides, Bar *et al.* [38] propose to use ℓ_1-norm in fidelity term, which is derived from Laplacian noise distribution. Cho *et al.* [39] develop a non-linear deconvolution model to handle saturated pixels and non-Gaussian noise.

When taking kernel estimation error into account, one common strategy is to decrease the trade-off parameter to over-strengthen the regularization term. This strategy, however, suppress the artifacts caused by inaccurate blur kernel at the cost of over-smooth restoration results. In contrast, the proposed partial deconvolution model modifies the fidelity term by taking kernel estimation error into account, and thus can better preserve textures while reducing artifacts. Moreover, besides the wavelet-based and learning-based deconvolution methods, partial deconvolution is flexible to incorporate with other deconvolution methods including gradient-based and patch-based ones.

B. Robust Deconvolution

Given the inaccurate blur kernel, several other works try to design specific priors rather than the natural image priors for reducing ringing artifacts. In [23] and [24], local smoothness constraint is adopted to force structure consistency of deblurred and blurry images. Yuan *et al.* [25] propose to iteratively impose bilateral regularization for recovering sharp edges. In [26], cross-channel priors are designed to reduce ringing effect. Besides, Mosleh *et al.* [33] propose a post-processing technique for ringing artifact removal, in which a set of Gabor filters with one-to-one correspondence to detected zero points in FS are constructed, and then their responses are imposed as the regularization on the restored image to reduce the ringing artifacts. Although the ringing effect can be relieved by these methods, other artifacts like color distortions caused by kernel estimation error still remain.

Currently, there is only one method to implicitly model kernel estimation error [27]. Rather than model the kernel error $\Delta\mathbf{k} = \mathbf{k}^{gt} - \mathbf{k}$, Ji and Wang [27] introduce an auxiliary variable as the image residual $\mathbf{r} = \Delta\mathbf{k} \otimes \mathbf{x}$ and impose ℓ_1-norm sparsity regularization on $\mathbf{r}$,

$$\min_{\mathbf{x},\mathbf{r}} \frac{\lambda}{2}\|\mathbf{k} \otimes \mathbf{x} + \mathbf{r} - \mathbf{y}\|^2 + \mathcal{R}(\mathbf{x}) + \tau\|\mathbf{r}\|_1, \tag{4}$$

which is solved by alternatively updating $\mathbf{x}$ and $\mathbf{r}$. To suppress the ringing artifact, they further explicitly separate sharp edges and periodic patterns with different sparsity-based priors. However, the image residual $\mathbf{r}$ intend to absorb more texture details from clean image $\mathbf{x}$, resulting in over-smoothed deblurring results.

Instead of imposing regularization on the residual image $\mathbf{r}$, the proposed partial deconvolution method explicitly models kernel estimation error in Fourier domain. Compared with [27], our model is more effective in suppressing the adverse effect of kernel estimation error while preserving more texture details.

III. Our Partial Deconvolution Model

In this section, we first formulate the partial deconvolution model in the Fourier domain, in which partial map is introduced to localize reliable Fourier coefficients of estimated blur kernel. Then, we develop an E-M framework to jointly update partial map and clean image. Finally, we provide an approach to estimate the reference FS.

A. Partial Deconvolution

Let us first assume that partial map $\mathbf{\Omega}$ is available to indicate reliable Fourier components $\mathbf{\Omega}_i = 1$ and the unreliable ones $\mathbf{\Omega}_i = 0$. Starting from the idea that unreliable Fourier coefficients should be excluded during deconvolution, we propose a new partial convolution model in the Fourier domain,

$$\mathcal{F}_{\mathbf{\Omega}}(\mathbf{y}) = \mathcal{F}_{\mathbf{\Omega}}(\mathbf{k} \otimes \mathbf{x}) + \mathcal{F}_{\mathbf{\Omega}}(\mathbf{n}), \tag{5}$$

where $\mathcal{F}_{\mathbf{\Omega}}$ is partial 2D Fourier transform under $\mathbf{\Omega}$, same as in the partial Fourier imaging [40], [41].

Also by the Bayes' theorem, the clean image $\mathbf{x}$ can be estimated as

$$\begin{aligned}\mathbf{x} &= \arg\max_{\mathbf{x}} \log \Pr(\mathbf{x}|\widehat{\mathbf{y}}, \mathbf{k}, \mathbf{\Omega}) \\ &= \arg\max_{\mathbf{x}} \log \Pr(\widehat{\mathbf{y}}|\mathbf{k}, \mathbf{x}, \mathbf{\Omega}) + \log \Pr(\mathbf{x}),\end{aligned} \tag{6}$$

where $\widehat{\mathbf{y}} = \mathcal{F}(\mathbf{y})$. With the additive white Gaussian noise in the Fourier domain, the partial deconvolution model can be written as

$$\mathbf{x} = \arg\min_{\mathbf{x}} \frac{\lambda}{2} \|\mathcal{F}_{\mathbf{\Omega}}(\mathbf{k} \otimes \mathbf{x}) - \mathcal{F}_{\mathbf{\Omega}}(\mathbf{y})\|^2 + \mathcal{R}(\mathbf{x}). \tag{7}$$

One can see that if the blur kernel is accurate, each entry of the partial map $\mathbf{\Omega}$ would be 1, and the partial deconvolution is exactly equivalent to the conventional deconvolution model in Eqn. (3). Otherwise, only the reliable Fourier entries, *i.e.*, $\mathbf{\Omega}_i = 1$, will be used during deconvolution, and the missing Fourier coefficients, *i.e.*, $\mathbf{\Omega}_i = 0$ are expected to be recovered [40], [41], resulting in the robust deblurring model.

B. E-M Framework for Partial Deconvolution

In the partial deconvolution model, the key issue is to determine the partial map $\mathbf{\Omega}$. We hereby develop an E-M framework [39], [42] for estimating the partial map and clean image alternatively. Currently, we assume that the reference FS is available at hand.

Therefore, let us again revisit the Bayes' estimation of clean image $\mathbf{x}$, and introduce a latent binary variable $\mathbf{\Omega}'$,

$$\begin{aligned}\mathbf{x} &= \arg\max_{\mathbf{x}} \Pr(\widehat{\mathbf{y}}|\mathbf{k}, \mathbf{x}) \Pr(\mathbf{x}) \\ &= \arg\max_{\mathbf{x}} \sum\nolimits_{\mathbf{\Omega}'} \Pr\left(\widehat{\mathbf{y}}, \mathbf{\Omega}'|\mathbf{k}, \mathbf{x}\right) \Pr(\mathbf{x}) \\ &= \arg\max_{\mathbf{x}} \sum\nolimits_{\mathbf{\Omega}'} \Pr\left(\widehat{\mathbf{y}}|\mathbf{\Omega}', \mathbf{k}, \mathbf{x}\right) \Pr\left(\mathbf{\Omega}'|\mathbf{k}, \mathbf{x}\right) \Pr(\mathbf{x}),\end{aligned} \tag{8}$$

where all the possible configurations of $\mathbf{\Omega}'$ should be collected, making the marginalization of $\Pr\left(\widehat{\mathbf{y}}, \mathbf{\Omega}'|\mathbf{k}, \mathbf{x}\right)$ intractable. So instead of marginalizing likelihood $\Pr\left(\widehat{\mathbf{y}}, \mathbf{\Omega}'|\mathbf{k}, \mathbf{x}\right)$ with respect to $\mathbf{\Omega}'$, the proposed E-M algorithm tries to evaluate the expectation of $\Pr\left(\widehat{\mathbf{y}}, \mathbf{\Omega}'|\mathbf{k}, \mathbf{x}\right)$, which is then used to find the optimal $\mathbf{x}$. Generally speaking, in the E-step, given the current estimation of clean image $\mathbf{x}_0$, the expectation $Q(\mathbf{x}, \mathbf{x}_0)$ of the log likelihood $\Pr\left(\widehat{\mathbf{y}}, \mathbf{\Omega}'|\mathbf{k}, \mathbf{x}\right)$ under $\Pr\left(\mathbf{\Omega}'|\widehat{\mathbf{y}}, \mathbf{k}, \mathbf{x}\right)$ can be estimated, where the posterior distribution $\Pr\left(\mathbf{\Omega}'|\widehat{\mathbf{y}}, \mathbf{k}, \mathbf{x}\right)$ should be first estimated by using $\mathbf{x}_0$ to approximate $\mathbf{x}$. Then in the subsequent M-step, the clean image $\mathbf{x}$ can be updated by minimizing the log posterior $Q(\mathbf{x}, \mathbf{x}_0) + \log \Pr(\mathbf{x})$. In the following, we give the details of the E-M framework.

1) E-Step: Given the current estimation of clean image $\mathbf{x}_0$, the expectation $Q(\mathbf{x}, \mathbf{x}_0)$ of the log likelihood $\Pr\left(\widehat{\mathbf{y}}, \mathbf{\Omega}'|\mathbf{k}, \mathbf{x}\right)$ w.r.t. latent variable $\mathbf{\Omega}'$ can be written as

$$\begin{aligned}Q(\mathbf{x}, \mathbf{x}_0) &= E\left[\log \Pr\left(\widehat{\mathbf{y}}, \mathbf{\Omega}'|\mathbf{k}, \mathbf{x}\right)\right] \\ &= E\left[\log \Pr\left(\widehat{\mathbf{y}}|\mathbf{\Omega}', \mathbf{k}, \mathbf{x}\right) + \log \Pr\left(\mathbf{\Omega}'|\mathbf{k}, \mathbf{x}\right)\right],\end{aligned} \tag{9}$$

where E is the expectation under $\Pr\left(\mathbf{\Omega}'|\mathbf{y}, \mathbf{k}, \mathbf{x}_0\right)$. First, we need to specify the definitions of $\Pr\left(\widehat{\mathbf{y}}|\mathbf{\Omega}', \mathbf{k}, \mathbf{x}\right)$ and $\Pr\left(\mathbf{\Omega}'|\mathbf{k}, \mathbf{x}\right)$.

By assuming the noise is with independent identical Gaussian distribution, we have $\Pr\left(\widehat{\mathbf{y}}|\mathbf{\Omega}', \mathbf{k}, \mathbf{x}\right) = \prod_i \Pr\left(\widehat{\mathbf{y}}_i|\mathbf{\Omega}', \mathbf{k}, \mathbf{x}\right)$, and define

$$\Pr\left(\widehat{\mathbf{y}}_i|\mathbf{\Omega}', \mathbf{k}, \mathbf{x}\right) = \begin{cases} G\left(\widehat{\mathbf{y}}_i; \widehat{\mathbf{f}}_i, \sigma\right), & \text{if } \mathbf{\Omega}'_i = 1, \\ C, & \text{else,} \end{cases} \tag{10}$$

where $\widehat{\mathbf{f}} = \mathcal{F}(\mathbf{k} \otimes \mathbf{x})$, C is a constant by assuming that the Fourier coefficients corresponding to kernel error are with uniform distribution, and $G(x; \mu, \sigma)$ is the Gaussian function defined as

$$G(x; \mu, \sigma) = \frac{1}{\sqrt{2\pi}\sigma} \exp\left(-\frac{(x-\mu)^2}{2\sigma^2}\right), \tag{11}$$

where μ and σ are mean and standard deviation.

As for $\Pr\left(\mathbf{\Omega}'|\mathbf{k}, \mathbf{x}\right)$, we also assume it is independent identically distributed. Given the current clean image $\mathbf{x}$, we can obtain the reference FS $|\widehat{\mathbf{k}(\mathbf{x})}|$, and the estimation method will be presented in Section III-D.

In this work, instead of continuous probability definition of $\Pr\left(\mathbf{\Omega}'|\mathbf{k}, \mathbf{x}\right)$, we simply adopt the truncated definition

$$\begin{aligned}\Pr\left(\mathbf{\Omega}'_i = 1|\mathbf{k}, \mathbf{x}\right) &= \Pr\left(\mathbf{\Omega}'_i = 1|\ |\widehat{\mathbf{k}}|, |\widehat{\mathbf{k}(\mathbf{x})}|\right) \\ &= \begin{cases} p, & \text{if } \varphi\left(|\widehat{\mathbf{k}}|_i, |\widehat{\mathbf{k}(\mathbf{x})}|_i\right) \geq \tau, \\ 0, & \text{else,} \end{cases}\end{aligned} \tag{12}$$

where p is the probability of the blur kernel accuracy, τ is a positive threshold, and $\varphi(a, b) = \exp\left(-(a-b)^2\right)$.

Although the reference FS is more accurate than that of estimated blur kernel, it still has some estimation errors compared with the groundtruth one. By adopting the truncated probability definition, reference FS estimation error can be tolerated by the threshold τ and accuracy probability p.

So by taking Eqns. (10) and (12) into Eqn. (9), we can rewrite the expectation as

$$\begin{aligned} Q(\mathbf{x}, \mathbf{x}_0) &\propto \sum\nolimits_i E[\mathbf{\Omega}_i'|\mathbf{y}, \mathbf{k}, \mathbf{x}_0] \log G\left(\widehat{\mathbf{y}}_i; \widehat{\mathbf{f}}_i, \sigma\right) \\ &\propto \sum\nolimits_i \frac{E\left[\mathbf{\Omega}_i'|\mathbf{y}, \mathbf{k}, \mathbf{x}_0\right]}{2\sigma^2} |\widehat{\mathbf{y}}_i - \widehat{\mathbf{f}}_i|^2, \end{aligned} \tag{13}$$

where

$$E\left[\mathbf{\Omega}_i'|\mathbf{y}, \mathbf{k}, \mathbf{x}_0\right] = \Pr\left(\mathbf{\Omega}_i' = 1|\mathbf{y}, \mathbf{k}, \mathbf{x}_0\right). \tag{14}$$

With the Bayes' theorem

$$\Pr\left(\mathbf{\Omega}_i'|\widehat{\mathbf{y}}_i, \mathbf{k}, \mathbf{x}_0\right) = \frac{\Pr\left(\widehat{\mathbf{y}}_i|\mathbf{\Omega}_i', \mathbf{k}, \mathbf{x}_0\right) \Pr\left(\mathbf{\Omega}_i'|\mathbf{k}, \mathbf{x}_0\right)}{\Pr\left(\widehat{\mathbf{y}}_i|\mathbf{k}, \mathbf{x}_0\right)}, \tag{15}$$

where

$$\Pr\left(\widehat{\mathbf{y}}_i|\mathbf{k}, \mathbf{x}_0\right) = \sum_{\mathbf{\Omega}_i'=0}^{1} \Pr\left(\widehat{\mathbf{y}}_i|\mathbf{\Omega}_i', \mathbf{k}, \mathbf{x}_0\right) \Pr\left(\mathbf{\Omega}_i'|\mathbf{k}, \mathbf{x}_0\right). \tag{16}$$

Again, by taking Eqns. (10) and (12) into account, we have

$$E\left[\mathbf{\Omega}_i'|\mathbf{y}, \mathbf{k}, \mathbf{x}_0\right] = \begin{cases} \dfrac{G\left(\widehat{\mathbf{y}}_i; \widehat{\mathbf{f}}_i, \sigma\right) p}{G\left(\widehat{\mathbf{y}}_i; \widehat{\mathbf{f}}_i, \sigma\right) p + C(1-p)}, & \text{if } \varphi\left(|\widehat{\mathbf{k}}|_i, |\widehat{\mathbf{k}(\mathbf{x}_0)}|_i\right) \geq \tau, \\ 0, & \text{else.} \end{cases} \tag{17}$$

To sum up, the E-step estimates the expectation of $\mathbf{\Omega}'$, which in the following is used as the partial map, *i.e.*, $\mathbf{\Omega}_i = E[\mathbf{\Omega}_i'|\mathbf{y}, \mathbf{k}, \mathbf{x}_0]$.

2) M-Step: Once the partial map $\mathbf{\Omega}$ is determined, the clean image $\mathbf{x}$ can be updated by

$$\begin{aligned} \mathbf{x} &= \arg\max_{\mathbf{x}} Q(\mathbf{x}, \mathbf{x}_0) + \log \Pr(\mathbf{x}) \\ &= \arg\min_{\mathbf{x}} \sum\nolimits_i \frac{\mathbf{\Omega}_i}{2\sigma^2} \left|\mathcal{F}(\mathbf{k} \otimes \mathbf{x})_i - \mathcal{F}(\mathbf{y})_i\right|^2 + \mathcal{R}(\mathbf{x}). \end{aligned} \tag{18}$$

By denoting $\frac{1}{\sigma^2}$ as λ, we reformulate the problem (18) as

$$\mathbf{x} = \arg\min_{\mathbf{x}} \frac{\lambda}{2} \|\mathbf{\Omega F K x} - \mathbf{\Omega F y}\|^2 + \mathcal{R}(\mathbf{x}), \tag{19}$$

where $\mathbf{x} \in \mathbb{R}^N$ denotes the vectorization of an image, $\mathbf{K} \in \mathbb{R}^{N \times N}$ is the blur matrix and $\mathbf{F} \in \mathbb{C}^{N \times N}$ is the Fourier transform matrix. As to partial map $\mathbf{\Omega}$, we also need to rearrange it as a $N \times N$ diagonal matrix, whose diagonal values are the estimated expectation in Eqn. (17). The partial deconvolution model (19) can be incorporated with a variety of non-blind deconvolution model by specifying the regularization term $\mathcal{R}(\mathbf{x})$, which will be elaborated in details in Section IV.

Algorithm 1 Partial Deconvolution Under E-M Framework

Input: blurry image $\mathbf{y}$, estimated blur kernel $\mathbf{k}$
Output: clean image $\mathbf{x}$

1: Initialize $\mathbf{\Omega}^{(0)} = \mathbf{1}$, $\mathbf{x}_0 = \mathbf{y}$
2: Input $(\mathbf{y}, \mathbf{k}, \mathbf{\Omega}^{(0)}, \mathbf{x}_0)$ to Algorithm 2 or Eqn. (34), and return $\mathbf{x}^{(0)}$
3: **for** $t = 1$ to T_{EM} **do**
4: $\quad \mathbf{x}_0 = \mathbf{x}^{(t-1)}$
5: $\quad$ Update the reference FS $|\widehat{\mathbf{k}(\mathbf{x}_0)}|$ using Eqn. (27)
6: $\quad$ ***E step***: Estimate partial map $\mathbf{\Omega}^{(t)}$ using Eqn. (17) or Eqn. (21)
7: $\quad$ ***M step***: Input $(\mathbf{y}, \mathbf{k}, \mathbf{\Omega}^{(t)}, \mathbf{x}_0)$ to Algorithm 2 or Eqn. (34), and return $\mathbf{x}^{(t)}$
8: **end for**
9: $\mathbf{x} = \mathbf{x}^{(t)}$

C. Adding Zero Points Into Partial Map

As in [33], zero points in FS of blur kernel intend to cause ringing effect, and a post-processing technique is further developed to relieve ringing effect. Therefore, we provide a variant of partial deconvolution model, in which zero points of FS are included in the partial map for the purpose of removing ringing effects. Following [33], we use morphological operator to detect zero points in FS, resulting in the coordinate set $\mathbf{O} = \{i|\ |\mathbf{k}|_i \text{ is a zero point}\}$. And thus the probability definition of $\Pr\left(\mathbf{\Omega}'|\mathbf{k}, \mathbf{x}\right)$ can be revised as

$$\begin{aligned} &\Pr\left(\mathbf{\Omega}_i' = 1|\mathbf{k}, \mathbf{x}\right) \\ &\quad = \Pr\left(\mathbf{\Omega}_i' = 1|\ |\widehat{\mathbf{k}}|, |\widehat{\mathbf{k}(\mathbf{x})}|\right) \\ &\quad = \begin{cases} p, & \text{if } \varphi\left(|\widehat{\mathbf{k}}|_i, |\widehat{\mathbf{k}(\mathbf{x})}|_i\right) \geq \tau\ \ \&i \notin \mathbf{O}, \\ 0, & \text{else.} \end{cases} \end{aligned} \tag{20}$$

and the expectation of partial map can be accordingly derived as

$$E\left[\mathbf{\Omega}_i'|\mathbf{y}, \mathbf{k}, \mathbf{x}_0\right] = \begin{cases} \frac{G(\widehat{\mathbf{y}}_i; \widehat{\mathbf{f}}_i, \sigma) p}{G(\widehat{\mathbf{y}}_i; \widehat{\mathbf{f}}_i, \sigma) p + C(1-p)}, & \text{if } \varphi\left(|\widehat{\mathbf{k}}|_i, |\widehat{\mathbf{k}(\mathbf{x}_0)}|_i\right) \geq \tau \& i \notin \mathbf{O}, \\ 0, & \text{else.} \end{cases} \tag{21}$$

In [33], once the zero points are detected, a set of Gabor filters, each corresponding to one zero point, are constructed, and are imposed as regularization to reduce the ringing effect. Since the computational complexity is proportional to the number of zero points, only several ones with low frequencies are used. However, in the proposed partial deconvolution model, rather than a post-processing technique in [33], zero points can be directly included in the partial map, and thus the de-ringing effect can be achieved during deconvolution. Besides, the complexity of our partial deconvolution is independent with the number of zero points. Thus all the detected zero points can be included into the partial map without increasing computational load.

In Algorithm 1, under the E-M alternations, the overall partial deconvolution algorithm is summarized for jointly estimating the partial map and clean image.

D. Estimating the Reference Fourier Spectrum

As for the reference FS $|\widehat{\mathbf{k}(\mathbf{x})}|$ in E-step, its best choice is definitely the ground truth one $|\widehat{\mathbf{k}^{gt}}|$. But as with the groundtruth blur kernel, its FS is also not available in practice. So we in this section propose an approach to estimate the reference FS from the blurry image.

On one hand, for a clean image $\mathbf{x}$ of natural scene, it is suggested that its Fourier spectrum follows the power law [28],

$$|\hat{\mathbf{x}}(\boldsymbol{\omega})|^2 \propto \|\boldsymbol{\omega}\|^{-2}, \tag{22}$$

where $\boldsymbol{\omega} = (\omega_1, \omega_2) \neq (0, 0)$ is the Fourier frequency coordinate. On the other hand, as for a second-order derivative filter, *e.g.*, $\mathbf{d} = [-1, -2, -1; -2, 12, -2; -1, -2, -1]$ used in this paper, its Fourier spectrum has the following approximation,

$$|\hat{\mathbf{d}}(\boldsymbol{\omega})|^2 \approx c\|\boldsymbol{\omega}\|^2, \tag{23}$$

where c is a constant. Therefore, for a blurry image $\mathbf{y}$ degraded by Eqn.(1), it is easy to derive that

$$\begin{aligned} |\widehat{\mathbf{d} \otimes \mathbf{y}}(\boldsymbol{\omega})|^2 &= |\hat{\mathbf{k}}(\boldsymbol{\omega})|^2 |\hat{\mathbf{d}}(\boldsymbol{\omega})|^2 |\hat{\mathbf{x}}(\boldsymbol{\omega})|^2 + 2\sigma^2 \\ &\approx c|\hat{\mathbf{k}}(\boldsymbol{\omega})|^2 \|\boldsymbol{\omega}\|^2 \|\boldsymbol{\omega}\|^{-2} + 2\sigma^2 \\ &= c|\hat{\mathbf{k}}(\boldsymbol{\omega})|^2 + 2\sigma^2, \end{aligned} \tag{24}$$

where σ is standard deviation of Gaussian noise. Thus in this ideal case, we can obtain the reference FS by

$$|\widehat{\mathbf{k}(\mathbf{x})}| = \sqrt{\frac{\mathcal{F}(\mathbf{d})\overline{\mathcal{F}(\mathbf{d})}\mathcal{F}(\mathbf{y})\overline{\mathcal{F}(\mathbf{y})} - 2\sigma^2}{c}}. \tag{25}$$

However, the power law in Eqn. (22) only holds for texture-only images, and is usually destroyed by salient structure in natural images. In [28], a weighted power law is proposed to restrain the structures for better FS estimation.

In this work, we propose a new approach to estimate FS from blurry image. As for an clean image $\mathbf{x}$, we separate it into structure $\mathbf{S}$ and texture $\mathbf{T}$, *i.e.*, $\mathbf{x} = \mathbf{S} + \mathbf{T}$, where the texture $\mathbf{T}$ holds the power law Eqn. (22). Thus, for frequency $\boldsymbol{\omega}$, we also have the approximation $c \approx |\hat{\mathbf{d}}(\boldsymbol{\omega})|^2 |\hat{\mathbf{T}}(\boldsymbol{\omega})|^2$, based on which Eqn. (24) can be refined as

$$\begin{aligned} &|\widehat{\mathbf{d} \otimes \mathbf{y}}(\boldsymbol{\omega})|^2 \\ &\quad\approx |\hat{\mathbf{k}}(\boldsymbol{\omega})|^2 \left(|\hat{\mathbf{d}}(\boldsymbol{\omega})|^2 |\hat{\mathbf{S}}(\boldsymbol{\omega})|^2 + |\hat{\mathbf{d}}(\boldsymbol{\omega})|^2 |\hat{\mathbf{T}}(\boldsymbol{\omega})|^2\right) + 2\sigma^2 \\ &\quad\approx |\hat{\mathbf{k}}(\boldsymbol{\omega})|^2 \left(|\hat{\mathbf{d}}(\boldsymbol{\omega})|^2 |\hat{\mathbf{S}}(\boldsymbol{\omega})|^2 + c\right) + 2\sigma^2. \end{aligned} \tag{26}$$

Therefore, the reference FS can be estimated by

$$|\widehat{\mathbf{k}(\mathbf{x})}| = \sqrt{\frac{\mathcal{F}(\mathbf{d})\,\overline{\mathcal{F}(\mathbf{d})}\mathcal{F}(\mathbf{y})\,\overline{\mathcal{F}(\mathbf{y})} - 2\sigma^2}{\mathcal{F}(\mathbf{d})\,\overline{\mathcal{F}(\mathbf{d})}\mathcal{F}(\mathbf{S})\,\overline{\mathcal{F}(\mathbf{S})} + c}}. \tag{27}$$

The reference FS is iteratively updated during E-M alterations. By providing the clean image $\mathbf{x}$ as the current estimation $\mathbf{x}_0$ in M-step, we employ relative total variation [43] to separate it into structure and texture. As for the constant c, we calculate it as the average power over all the frequencies of texture $\mathbf{T}$,

$$c = \frac{1}{N}\sum\nolimits_{\omega} \mathcal{F}(\mathbf{d})\,\overline{\mathcal{F}(\mathbf{d})}\mathcal{F}(\mathbf{T})\,\overline{\mathcal{F}(\mathbf{T})}, \tag{28}$$

where N is the number of pixels in texture image $\mathbf{T}$. Along with the E-M alternations, better update of clean image $\mathbf{x}$ will lead to better estimation of the reference FS, and vice versa.

The FS of blur kernel is much easier to estimate than blur kernel itself, and in [28], [30] the phases can be further recovered to reconstruct blur kernel, which has also achieved comparable performance compared with MAP-based and VB-based state-of-the-art blind deconvolution methods [3], [10], [12], [44], [45]. In this work, we only use the estimated FS as the reference to indicate the reliability of estimated blur kernel, which is more well conditioned than blur kernel estimation.

E. Discussion

The proposed partial deconvolution model is formulated in the Fourier domain, and when each entry in partial map is 1, it is exactly equivalent to the conventional deconvolution model. The expectation of partial map $\boldsymbol{\Omega}$ actually serves as a metric matrix whose entries are ranged in [0, 1], measuring the reliability of each Fourier component. When $\boldsymbol{\Omega}_i$ approaches to 1, the i-th Fourier component of blur kernel is reliable, and will contribute more to the deconvolution. When $\boldsymbol{\Omega}_i$ approaches to 0, its corresponding component will be ruled out, making the deconvolution result free from the adverse effect of kernel estimation error. Also, along with the deconvolution quality improvement, the more accurate clean image will lead to better reference FS estimation, which will mutually facilitate subsequent clean image estimation.

The proposed model has commonality in essence with the partial Fourier imaging model, where the latent image is recovered from its partially sampled Fourier coefficients. In the proposed partial deconvolution model, the partial map $\boldsymbol{\Omega}$ works as the sampling matrix in partial Fourier imaging problem. If the sampling matrix satisfies the restricted isometry property (RIP) [40], [41], the latent image can be successfully recovered with a high probability. The partial map $\boldsymbol{\Omega}$ in partial deconvolution model changes during E-M alternations, and the number of non-zero entries in $\boldsymbol{\Omega}$ should also be sufficiently large to guarantee the high probability of correct recovery of Fourier spectrum. The extensive results in Section V experimentally validate the feasibility of the partial deconvolution model.

IV. Incorporation With Deconvolution Methods

In the M-step, given the partial map $\boldsymbol{\Omega}$, the deconvolution step can be realized by specifying $\mathcal{R}(\mathbf{x})$, and can be applied in various deconvolution models. In this section, we take wavelet-based and learning-based models as examples to show how to apply partial deconvolution for robust deblurring.

A. Partial Deconvolution in Wavelet-Based Model

In this subsection, we take the frame-based wavelet [31] in synthesis form for partial deconvolution (PDW), formulated as

$$\mathbf{c} = \arg\min_{\mathbf{c}} \frac{\lambda}{2}\left\|\boldsymbol{\Omega}\mathbf{F}\mathbf{K}\mathbf{W}^T\mathbf{c} - \boldsymbol{\Omega}\mathbf{F}\mathbf{y}\right\|^2 + \|\mathbf{c}\|_1, \tag{29}$$

Algorithm 2 PDW

Input: blurry image $\mathbf{y}$, blur kernel $\mathbf{k}$, partial map $\mathbf{\Omega}$, initial clean image $\mathbf{x}^{(0)}$
Output: clean image $\mathbf{x}$
1: $s^{(1)}=1$, $\mathbf{c}^{(0)}=\mathbf{W}\mathbf{x}^{(0)}$, $\mathbf{u}^{(1)}=\mathbf{c}^{(0)}$
2: **for** $t=1$ to T_{APG} **do**
3: $\quad\mathbf{z}^{(t)}=\mathbf{u}^{(t)}-\frac{1}{L_f}\nabla f_S\left(\mathbf{u}^{(t)}\right)$
4: $\quad\mathbf{c}^{(t)}=\arg\min_{\mathbf{c}}\left\{\frac{L_f}{2}\left\|\mathbf{c}-\mathbf{z}^{(t)}\right\|^2+\|\mathbf{c}\|_1\right\}$
5: $\quad s^{(t+1)}=\frac{1+\sqrt{1+4(s^{(t)})^2}}{2}$
6: $\quad\mathbf{u}^{(t+1)}=\mathbf{u}^{(t)}+\frac{s^{(t)}-1}{s^{(t+1)}}\left(\mathbf{c}^{(t)}-\mathbf{c}^{(t-1)}\right)$
7: **end for**
8: $\mathbf{x}=\mathbf{W}^T\mathbf{c}^{(t)}$

where $\mathbf{W}$ is the wavelet transform bases, the clean image $\mathbf{x}$ can be represented by the wavelet coefficients $\mathbf{c}$ under $\mathbf{W}$.

We employ the accelerated proximal gradient (APG) algorithm, which has been widely used in image restoration methods, e.g., FISTA [46] and GAPG [47], to solve this problem. By setting $f_S(\mathbf{c})=\frac{\lambda}{2}\left\|\mathbf{\Omega}\mathbf{F}\mathbf{K}\mathbf{W}^T\mathbf{c}-\mathbf{\Omega}\mathbf{F}\mathbf{y}\right\|^2$. Instead of directly minimizing (29), APG algorithm decomposes it into a sequence of quadratic subproblems at chosen points $\mathbf{u}^{(t)}$, which can be written as

$$\min_{\mathbf{c}}\frac{L_f}{2}\|\mathbf{c}-\mathbf{u}^{(t)}\|^2+\left\langle\nabla f_S(\mathbf{u}^{(t)}),\mathbf{c}-\mathbf{u}^{(t)}\right\rangle+\|\mathbf{c}\|_1, \tag{30}$$

where L_f is the Lipschitz constant of ∇f_S, and its value can be set based on $\|f_S(\mathbf{u}_1)-f_S(\mathbf{u}_2)\|\le L\|\mathbf{u}_1-\mathbf{u}_2\|$. The gradient $\nabla f_S\left(\mathbf{u}^{(t)}\right)$ can be written as

$$\nabla f_S(\mathbf{u})=\lambda\mathbf{W}\mathbf{K}^T\mathbf{F}^T\mathbf{\Omega}^T\left(\mathbf{\Omega}\mathbf{F}\mathbf{K}\mathbf{W}^T\mathbf{u}^{(t)}-\mathbf{\Omega}\mathbf{F}\mathbf{y}\right). \tag{31}$$

The matrix multiplication can be efficiently computed in Fourier domain, and the fast wavelet transform implementation.

And the proximal subproblem is simply an ℓ_1-norm minimization problem,

$$\mathbf{c}=\arg\min_{\mathbf{c}}\frac{L_f}{2}\|\mathbf{c}-\mathbf{z}\|^2+\|\mathbf{c}\|_1, \tag{32}$$

where $\mathbf{z}^{(t)}=\mathbf{u}^{(t)}-\frac{1}{L_f}\nabla f_S(\mathbf{u}^{(t)})$, and it can be solved by soft-thresholding operation [14]. Finally when the wavelet representation $\mathbf{c}$ has been optimized, clean image $\mathbf{x}$ can be recovered by $\mathbf{x}=\mathbf{W}^T\mathbf{c}$.

The overall PDW algorithm can be summarized as Algorithm 2.

B. Partial Deconvolution in Learning-Based Model

Recently, the discriminative learning-based method has arisen in image restoration applications and achieved superior performance [48]–[50]. We hereby show that the partial deconvolution can also be applied in the discriminative learning-based model (PDL).

By specifying the regularization term $\mathcal{R}(\mathbf{x})$ as fields of experts (FoE) [32] to learn the distribution of natural images, the partial deconvolution model can be formulated as

$$\min_{\mathbf{x}}\frac{\lambda}{2}\|\mathcal{F}_\Omega(\mathbf{y})-\mathcal{F}_\Omega(\mathbf{k}\otimes\mathbf{x})\|^2+\sum_{j=1}^{N}\sum_{i=1}^{N_r}\mathcal{R}_i\left((\mathbf{p}_i\otimes\mathbf{x})_j\right), \tag{33}$$

where $\mathbf{p}_i$ is linear filters with diverse patterns to extract information from natural images, and $\mathcal{R}_i$ is non-linear transform. Due to its powerful expression, the regularization has been recently applied in discriminative learning for a variety of image restoration tasks [22], [37], [51], e.g., Gaussian denoising, JPEG deblocking, super-resolution, where efficiency and effectiveness can be concurrently guaranteed.

Due to the high non-convexity of the optimization problem Eqn. (33), it is difficult to solve it in closed-form, and we instead use the gradient descent method. Given the parameters $\Theta^{(t)}=\{\lambda^{(t)},\mathbf{p}_i^{(t)},\mathcal{R}_i^{(t)}\}_{i=1}^{N_r}$ for stage t where N_r is the number of filters and non-linear transforms, the clean image is updated by

$$\begin{aligned}\mathbf{x}^{(t)}=\mathbf{x}^{(t-1)}&-\sum_{i=1}^{N_r}\mathbf{P}_i^{(t)\mathrm{T}}\mathcal{R}_i^{(t)'}(\mathbf{P}_i^{(t)}\mathbf{x}^{(t-1)})\\&-\lambda^{(t)}\mathbf{K}^{\mathrm{T}}\mathbf{F}^{\mathrm{T}}\mathbf{\Omega}^{\mathrm{T}}\left(\mathbf{\Omega}\mathbf{F}\mathbf{K}\mathbf{x}^{(t-1)}-\mathbf{\Omega}\mathbf{F}\mathbf{y}\right).\end{aligned} \tag{34}$$

The parameters $\Theta^{(t)}=\{\lambda^{(t)},\mathbf{p}_i^{(t)},\mathcal{R}_i^{(t)}\}_{i=1}^{N_r}$ can be learned under the discriminative learning framework. Given the training set $\{\mathbf{x}_s^{gt},\mathbf{y}_s,\mathbf{k}_s\}_{s=1}^{S}$, where S is the number of training images, the parameter for stage t can be learned by solving a bi-level optimization problem,

$$\begin{aligned}&\Theta^{(t)}\\&=\arg\min_{\Theta}\mathcal{L}(\Theta)=\sum_{s=1}^{S}\frac{1}{2}\left\|\mathbf{x}_s^{(t)}-\mathbf{x}_s^{gt}\right\|^2\\&\quad s.t.\ \mathbf{x}_s^{(t)}=\mathbf{x}_s^{(t-1)}-\sum_{i=1}^{N_r}\mathbf{P}_i^{(t)\mathrm{T}}\mathcal{R}_i^{(t)'}(\mathbf{P}_i^{(t)}\mathbf{x}_s^{(t-1)})\\&\qquad\qquad-\lambda^{(t)}\mathbf{K}^{\mathrm{T}}\mathbf{F}^{\mathrm{T}}\mathbf{\Omega}^{(t)\mathrm{T}}\left(\mathbf{\Omega}^{(t)}\mathbf{F}\mathbf{K}\mathbf{x}_s^{(t-1)}-\mathbf{\Omega}^{(t)}\mathbf{F}\mathbf{y}_s\right).\end{aligned} \tag{35}$$

As suggested in [22], [51], the non-linear transform $\mathcal{R}_i'$ can be parameterized as mixture of Gaussian RBFs,

$$\mathcal{R}_i'(z)=\sum_{j=1}^{M}\pi_{ij}\exp\left(-\frac{\gamma}{2}(z-\mu_j)^2\right), \tag{36}$$

which is the combination of M Gaussian RBF kernels with precision factor γ and mean value μ_j, and π_{ij} is the combination coefficients.

Once the non-linear function is parameterized, the parameters for stage t are $\Theta^{(t)}=\{\lambda^{(t)},\mathbf{p}_i^{(t)},\boldsymbol{\pi}_i^{(t)}\}_{i=1}^{N_r}$, whose gradient can be computed by the chain rule. Then the gradient-based LBFGS method can be used to learn parameters for each stage, and end-to-end training is utilized to further jointly fine tune all the parameters over stages.

C. Implementation

The p value indicating the accuracy of kernel is set as 0.96, and C is set as 0.01. As for the threshold τ, we adopt an

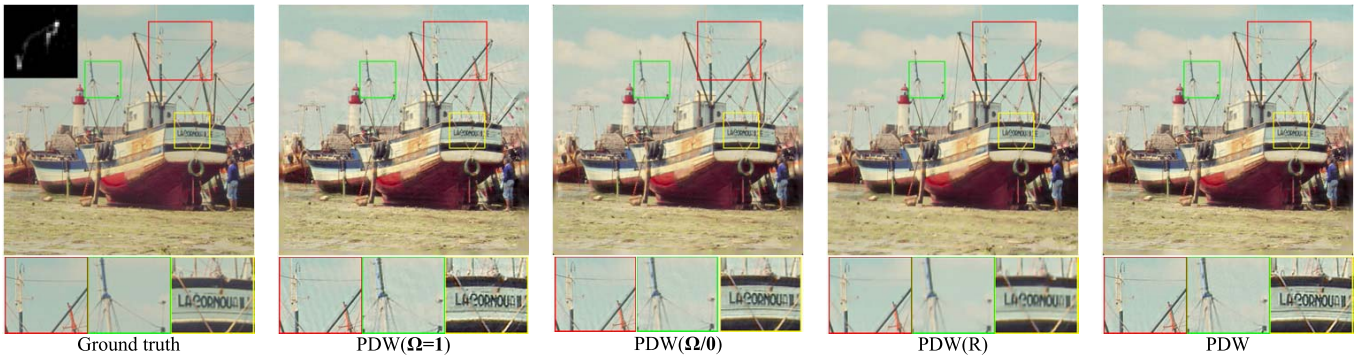

Fig. 3. Components analysis of PDW and its variants. In the sky close-ups, PDW($\mathbf{\Omega} = \mathbf{1}$) generates significant ringing effects, while the results by PDW and PDW($\mathbf{\Omega}/\mathbf{0}$) are visually plausible due to the partial deconvolution. Besides, the result by PDW(R) is over-smoothed due to the 30% lost entries in random partial map.

adaptive strategy. Let $\tau_{min} = \min_i \varphi(|\widehat{\mathbf{k}}|_i, |\widehat{\mathbf{k}(\mathbf{x})}|_i)$, and we set

$$\tau = \min\left(1, \tau_{min} + \frac{0.1}{\exp(5\tau_{min})}\right). \tag{37}$$

Thus, more inaccurate the blur kernel is, more entries will be ruled out. Along with the increase of τ_{min}, τ should have smaller gain than τ_{min}, indicating that blur kernel is more accurate.

As for PDW, the iteration number T_{EM} in the E-M alternations is set as 8. In the APG algorithms, the iteration number T_{APG} is set as 50, and the Lipschitz constant L_f is fixed as a relatively large value 3 to guarantee the convergence. As for PDL, the iteration number T_{EM} in of the E-M alternations is set as 15, and thus the PDL contains 16 stages where each entry in $\mathbf{\Omega}$ for the first stage is fixed as 1. We utilize $N_r = 24$ non-linear transform and linear filters with size 5×5, and the number of Gaussian RBFs is set as $M = 63$.

V. Experimental Results

In this section, we evaluate the partial deconvolution methods. First, to validate the effectiveness of the partial deconvolution model, we take PDW as an example to quantitatively evaluate PDW and its variants, analyzing the contribution of each component to the robust deblurring. Also PDW is compared with several state-of-the-art deblurring algorithms. Then, on two standard test datasets, given blur kernels estimated by some blind deconvolution methods, the proposed methods are compared with two state-of-the-art non-blind deconvolution methods, assessed in terms of both quantitative metrics and running time. The algorithm running time is recorded on a computer with 4.00GHz Intel(R) Core(TM) i7-6700K CPU. Finally, the proposed partial deconvolution method is applied to real blurry images.

A. Validation of Partial Deconvolution Model

We construct a synthetic dataset, in which ten 512×512 images and eight blur kernels [2] are used to generate synthetic blurred images, shown as Fig. 4. For all the blurred images, the Gaussian noise with $\sigma = 0.5$ was added. First, we analyze the contribution of each component in PDW, and then PDW is evaluated on the synthetic dataset compared with competing algorithms.

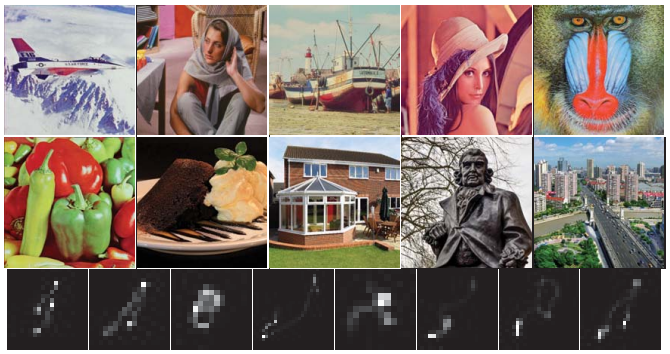

Fig. 4. Ten test images and eight blur kernels.

TABLE I
Average PSNR Values of PDW and Its Variants on the Synthetic Dataset

	Levin *et al.* [52]	Krishnan *et al.* [3]	Sun *et al.* [45]
PDW($\mathbf{\Omega} = \mathbf{1}$)	19.02	19.75	21.80
PDW($\mathbf{\Omega}/\mathbf{0}$)	19.19	19.87	21.82
PDW(R)	19.01	19.70	21.66
PDW	19.38	19.97	21.92

1) Component Analysis: On the synthetic dataset, we report the performance of PDW and its two variants, including PDW($\mathbf{\Omega}/\mathbf{0}$) in which zero points are not added into partial map, and PDW($\mathbf{\Omega} = \mathbf{1}$) that is equivalent to the conventional deconvolution model.

Table I reports the average PNSR comparison of variants of PDW. One can see that the partial map contributes more to the PSNR gain, while performance gain by adding zero points is very small. In kernel error free deconvolution, spectrum zero points are the main source of ringing effects [33] due to the entry-wise division in Fourier domain. However, as to deconvolution with inaccurate blur kernel, blur kernel estimation error can cause not only ringing effects but also other artifacts like color distortion, much exceeding the adverse effects of spectrum zero points. As for the visual quality, Fig. 3 shows an restoration example, where Levin *et al.*'s method [52] is

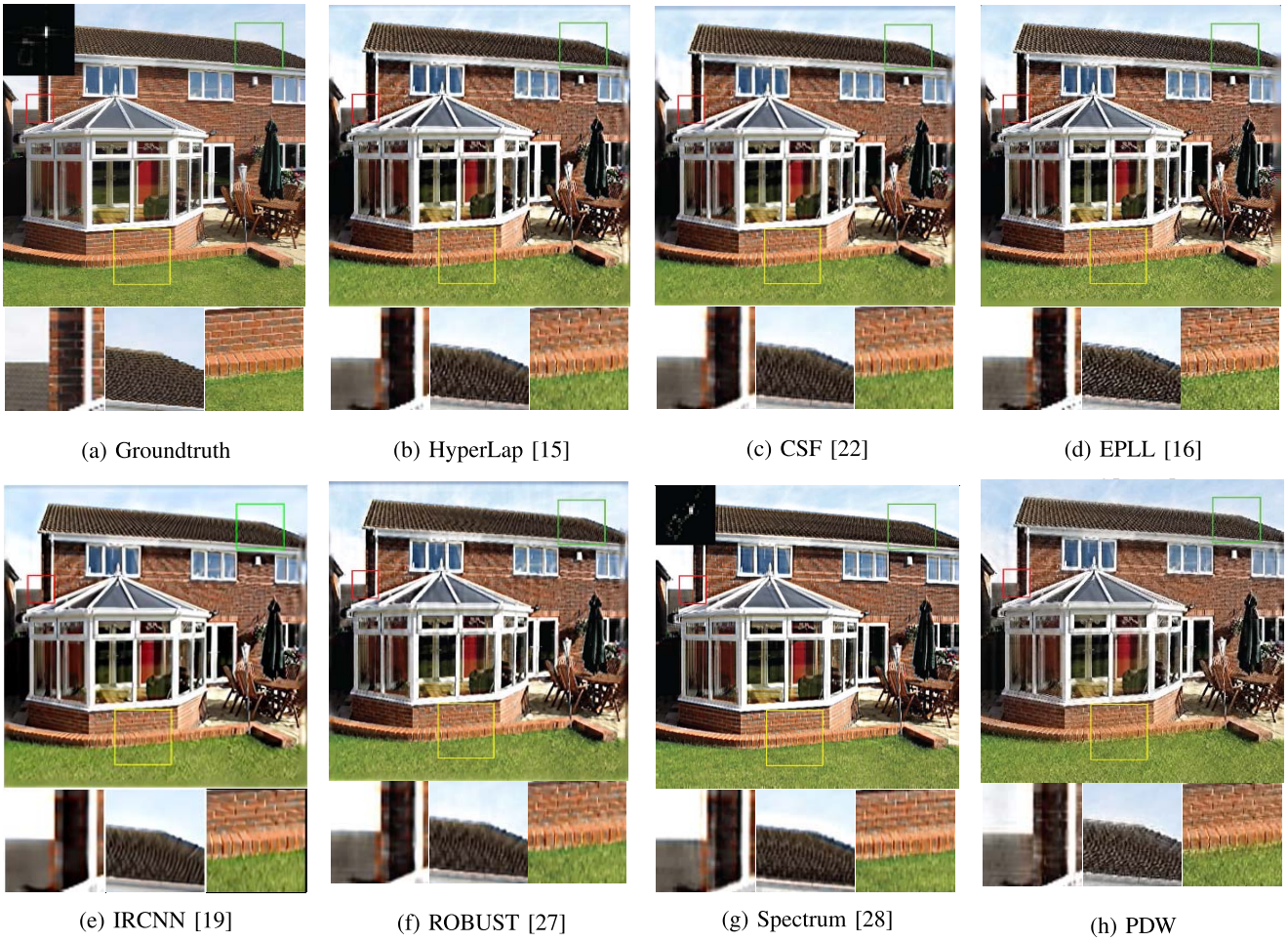

(a) Groundtruth (b) HyperLap [15] (c) CSF [22] (d) EPLL [16]

(e) IRCNN [19] (f) ROBUST [27] (g) Spectrum [28] (h) PDW

Fig. 5. Example of deblurred results on synthetic blurred image. Except (g) Spectrum [28] estimating blur kernel itself, all the non-blind deconvolution methods *i.e.*, (b)-(f) and (h), use the same blur kernel as input estimated by Krishnan *et al.* [15] shown in (a).

used to estimate blur kernel. The kernel estimation error is visible compared with the groundtruth one, and will severely cause artifacts. With the partial map, PDW and PDW($\mathbf{\Omega}/\mathbf{0}$) can both obtain much more visually plausible results than the conventional one PDW($\mathbf{\Omega} = \mathbf{1}$), indicating the effectiveness of the partial deconvolution. Moreover, the results by PDW and PDW($\mathbf{\Omega}/\mathbf{0}$) are less distinguishable, which indicates that the partial map contributes more to the performance gain than the zero points in FS. Besides, it is interesting to provide a variant of PDW with random partial map, i.e., PDW(R), whose 30% entries of partial map are randomly set as 0. Its performance is inferior to PDW in terms of both quantitative PSNR and visual quality. Due to the lost frequency information, the deblurred result of PDW(R) intends to be over-smoothing.

2) Comparison With Competing Algorithms: To quantitatively evaluate the performance of PDW, we compare it with several non-blind deconvolution methods, including gradient-based methods: FTVd [14], HyperLap [15]; filter-based method: CSF [22]; patch-based method: EPLL [16]; CNN-based method: IRCNN [19] and the method for handling kernel error: ROBUST [27]. To estimate the blur kernels, we apply three blind deconvolution methods, including VB-based method: Levin *et al.* [52], MAP-based method: Xu & Jia [44], patch-based method: Sun *et al.* [45].

TABLE II

AVERAGE PSNR COMPARISONS WITH COMPETING ALGORITHMS. THE BLUR KERNELS ARE ESTIMATED BY THREE BLIND DECONVOLUTION METHODS

	Levin *et al.* [52]	Krishnan *et al.* [3]	Sun *et al.* [45]
FTVd [14]	18.63	19.42	21.64
HyperLap [15]	18.66	19.53	21.71
CSF [22]	19.08	19.79	21.80
EPLL [16]	19.05	19.80	21.81
IRCNN [19]	19.26	19.86	21.95
ROBUST [27]	19.11	19.82	21.80
PDW	19.38	19.97	21.92
Spectrum [28]	20.07		

Table II reports the average PSNR comparison of these competing methods. Compared with conventional methods, one can see that PDW achieves the best average PSNR values. Fig. 5 shows the visual quality comparison. In the red close-up, the deblurring results by all the other competing methods suffer from the color distortion, while PDW achieves much superior visual quality. Moreover, since the image residual in ROBUST [27] absorbs more textures, its deblurring result is over-smoothed, while PDW can recover more detailed textures. Considering the CNN-based method, i.e., IRCNN [19],

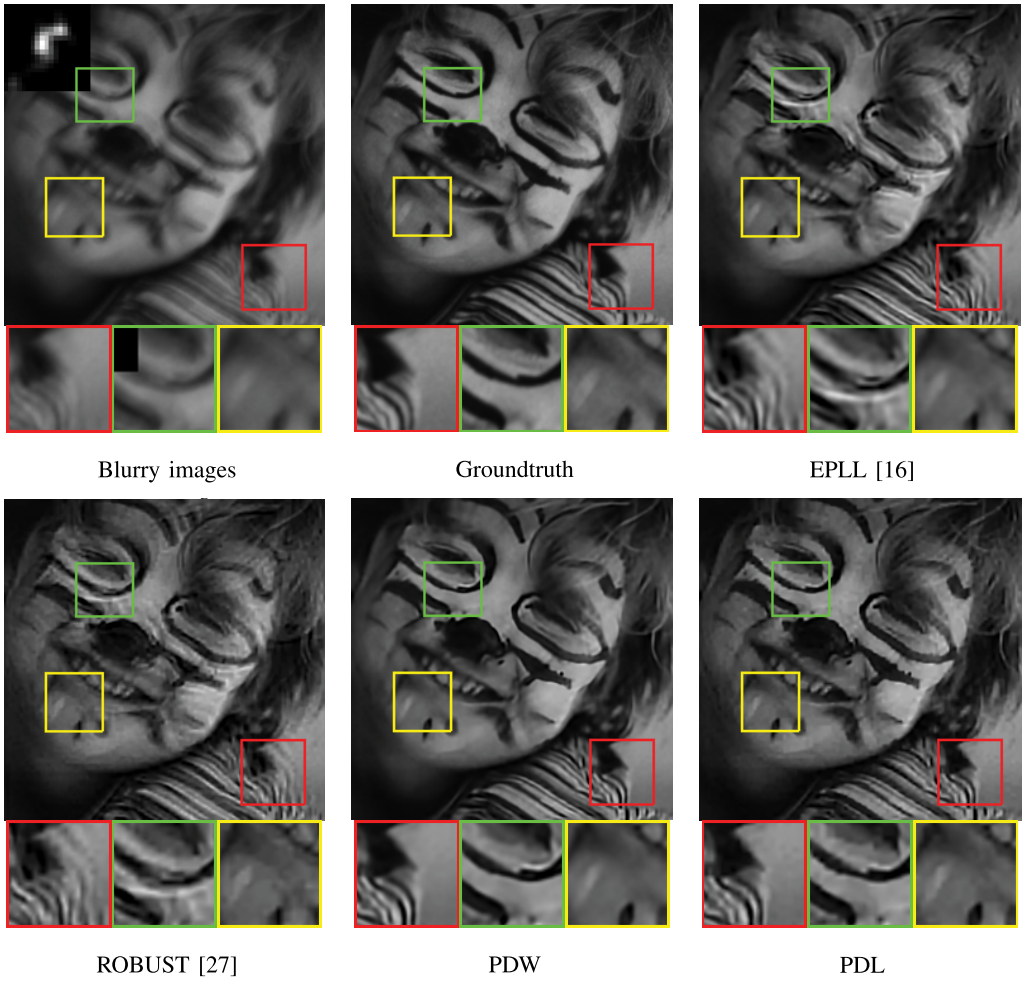

Fig. 6. Example of deblurred results on Levin *et al.*'s dataset [2]. The blur kernel is estimated by Cho&Lee [29].

PDW is a little inferior only for Sun et al. [45]. When the kernel estimation error is severe, e.g., for Krishnan et al., CNN denoisers should be strengthened to weaken the adverse effects of kernel error, and yield over-smoothed results as shown in Fig. 5. Furthermore, CNN priors in IRCNN can also be incorporated into our partial deconvolution model.

Besides, we report the results of Spectrum-based blind deconvolution [28] method, in which both blur kernel estimation and non-blind deconvolution are just ran as they are. On our constructed synthetic dataset, Spectrum-based method achieves PSNR 20.07dB that is higher than Levin *et al.* [2] and Krishnan *et al.* [3]. The comparable performance can be contributed to the well conditioned Fourier spectrum estimation. But the phase retrieval is too ill-posed to produce the best restoration quality. As shown in Fig. 5, more severe kernel estimation error by Spectrum-based method yields more visible ringing and distortion. Thus, we in this paper conclude that it is a better solution to employ Fourier spectrum as a reference for non-blind deconvolution to recover high quality clean image, with some good blind deconvolution method such as Sun *et al.* providing estimated blur kernel.

B. Evaluation on Synthetic Datasets

In this subsection, we further evaluate PDW and PDL on two standard test datasets. To train PDL, we need to construct the training dataset. The blurry images were generated from 100 clean images in the BSD dataset [54] by convolving with 8 blur kernels [2], and then Gaussian noise with $\sigma = 0.25$ were added. To save computational time, we used two optimized executable programs for blind deconvolution to estimate blur kernels, *i.e.*, Cho&Lee [29] and Xu&Jia [44]. So we have 1600 training samples, and we further select 500 samples with error ratio [2] above 3 to guarantee the quality of training samples. In the following comparison, the proposed methods are only compared with two competing deblurring algorithms, *i.e.*, EPLL [16] and ROBUST [27].

On the two test datasets, *i.e.*, Levin *et al.*'s dataset [2] and Kohler *et al.*'s dataset [53], PDW and PDL are compared with EPLL [16] and ROBUST [27]. Tables III and IV report the average PSNR comparison on Levin *et al.*'s dataset, and Kohler *et al.*'s dataset, respectively. PDW and PDL both achieve better results than the competing algorithms, especially PDL achieves the highest average PSNR. In terms of visual quality, Fig. 6 shows a deblurred example on

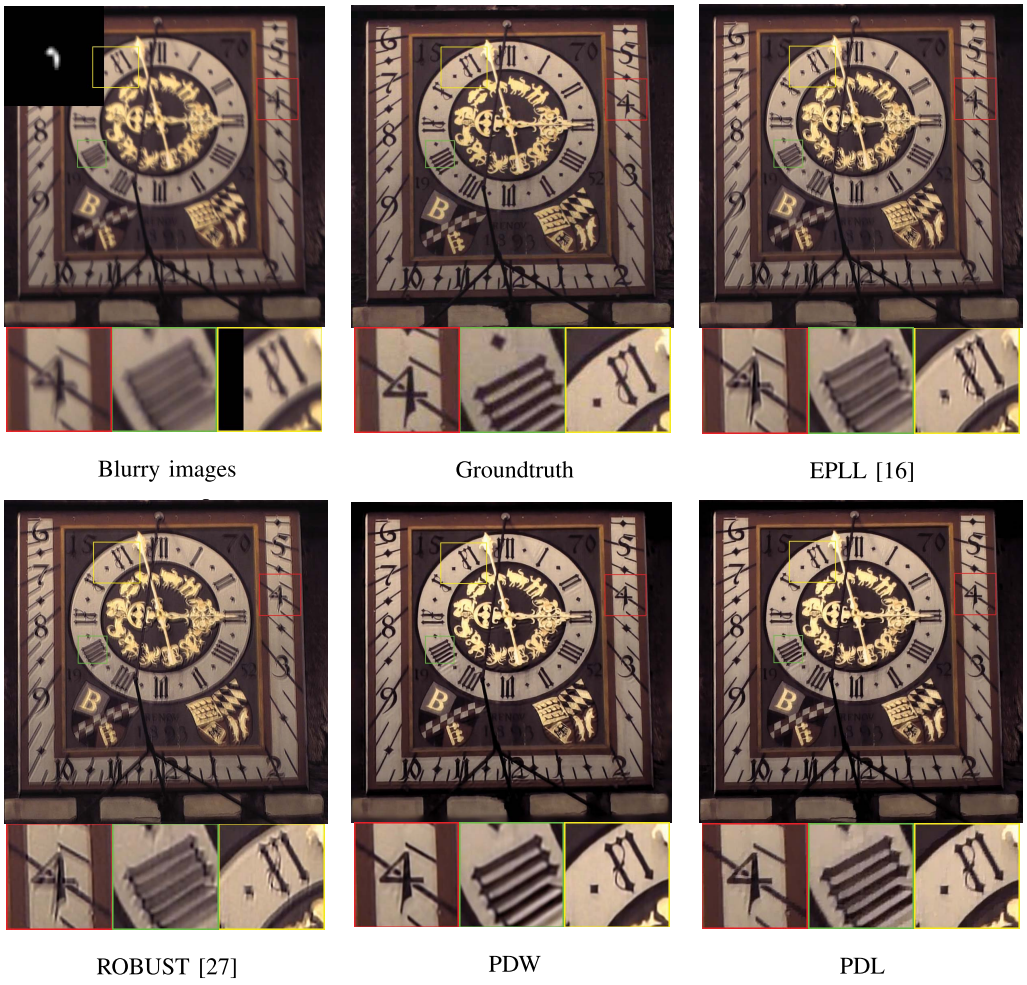

Fig. 7. Example of deblurred results on Kohler *et al.*'s dataset [53]. The blur kernel is estimated by Xu&Jia [44].

TABLE III

AVERAGE PSNR COMPARISON OF DEBLURRING RESULTS ON LEVIN *et al.*'S DATASET INCLUDING 4 CLEAN IMAGES AND 8 BLUR KENRELS. WE ALSO REPORT THE AVERAGE RUNNING TIME

	EPLL [16]	ROBUST [27]	PDW	PDL
Cho&Lee [29]	28.83	28.79	28.92	29.27
Xu&Jia [44]	29.45	29.37	29.31	29.55
CPU time (*sec.*)	127.1	59.73	61.14	2.183

TABLE IV

PSNR COMPARISON OF DEBLURRING RESULTS ON KOHLER *et al.*'S DATASET INCLUDING 4 CLEAN IMAGES AND 12 BLUR KERNELS, AND BLUR KERNELS ARE ESTIMATED BY XU&JIA [44]

Method	#1	#2	#3	#4	Avg.
EPLL [16]	31.64	26.64	31.45	28.42	29.53
ROBUST [27]	31.49	26.45	31.68	28.30	29.48
PDW	31.63	26.56	31.70	28.38	29.56
PDL	31.54	26.53	31.96	28.33	29.59

Levin *et al.*'s dataset. One can see that the results by PDW and PDL suffer less ringing effects, and PDL recovers more details than the other methods. From the example on Kohler *et al.*'s dataset shown in Fig. 7, one can draw the similar conclusion that the partial deconvolution contributes to the artifacts removal, and more detailed textures can be recovered. We also note that blurry images in Kohler *et al.*'s dataset are with mildly spatially variant blur.

We also report the running time on Levin *et al.*'s dataset in Table III. PDW is based on wavelet sparsity as ROBUST, but has extra computational cost for estimating partial map. Thus PDW is a little inefficient than ROBUST, but is two times faster than EPLL. Meanwhile, PDL is much more efficient than all the other competing algorithms.

C. Evaluation on Real Blurry Images

On real blurry images, we used Sun *et al.*'s method [45] to estimate blur kernels. We report the deblurring results by PDW compared with EPLL [16] and ROBUST [27]. Fig. 8 shows that the deblurring results by PDW significantly achieve much more visually plausible quality, with less distortions and ringing effects. For the first image, the texts recovered by PDW suffer from less ringing artifacts than EPLL and ROBUST. For the second image, the *eye* recovered by both EPLL and ROBUST has severe distortion, while the result by PDW is more visually plausible. For the third image, the result by PDW also has less artifacts than EPLL and ROBUST.

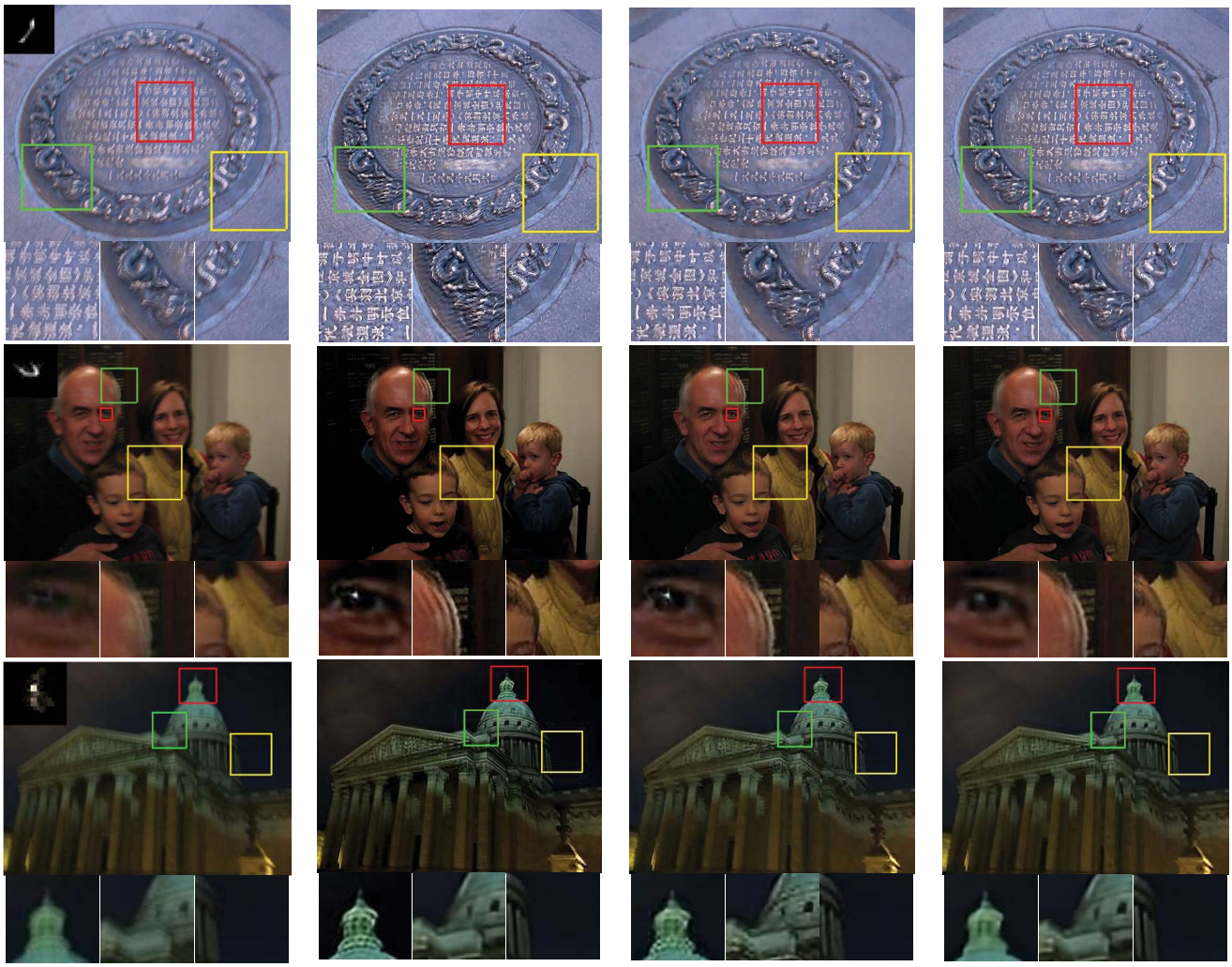

Fig. 8. Deblurred results on real blurry images. The blur kernels are all estimated by Sun *et al.* [45].

VI. Conclusion

In this paper, we proposed a novel partial deconvolution model, in which the deconvolution is partially performed with the reliable Fourier coefficients within the partial map. An E-M framework was developed to update the partial map and clean image alternatively. The proposed partial deconvolution can be incorporated into the existing deconvolution models for robust deblurring, and we give two examples, *i.e.*, the wavelet-based and learning-based deconvolution methods. With the partial deconvolution model, the adverse effect of kernel estimation error can be suppressed. Compared with state-of-the-art non-blind deconvolution methods, the partial deconvolution methods are able to relieve not only ringing effects but also other distortions. In blind deconvolution, blur kernel estimation error generally is inevitable, and in future work we will study the incorporation of CNN priors into partial deconvolution model for possible further improvement, and investigate more powerful modeling on inaccurate blur kernel for robust deblurring.

References

[1] T. F. Chan and C.-K. Wong, "Total variation blind deconvolution," *IEEE Trans. Image Process.*, vol. 7, no. 3, pp. 370–375, Mar. 1998.

[2] A. Levin, Y. Weiss, F. Durand, and W. T. Freeman, "Understanding and evaluating blind deconvolution algorithms," in *Proc. IEEE Conf. Comput. Vis. Pattern Recognit. (CVPR)*, Jun. 2009, pp. 1964–1971.

[3] D. Krishnan, T. Tay, and R. Fergus, "Blind deconvolution using a normalized sparsity measure," in *Proc. IEEE Conf. Comput. Vis. Pattern Recognit. (CVPR)*, Jun. 2011, pp. 233–240.

[4] D. Wipf and H. Zhang, "Revisiting Bayesian blind deconvolution," *J. Mach. Learn. Res.*, vol. 15, no. 1, pp. 3595–3634, Jan. 2014.

[5] G. Liu, S. Chang, and Y. Ma, "Blind image deblurring using spectral properties of convolution operators," *IEEE Trans. Image Process.*, vol. 23, no. 12, pp. 5047–5056, Dec. 2014.

[6] J. Pan, D. Sun, H. Pfister, and M.-H. Yang, "Blind image deblurring using dark channel prior," in *Proc. IEEE Conf. Comput. Vis. Pattern Recognit. (CVPR)*, Jun. 2016, pp. 1628–1636.

[7] D. Gong, M. Tan, Y. Zhang, A. Van den Hengel, and Q. Shi, "Blind image deconvolution by automatic gradient activation," in *Proc. IEEE Conf. Comput. Vis. Pattern Recognit. (CVPR)*, Jun. 2016, pp. 1827–1836.

[8] W. Ren, X. Cao, J. Pan, X. Guo, W. Zuo, and M.-H. Yang, "Image deblurring via enhanced low-rank prior," *IEEE Trans. Image Process.*, vol. 25, no. 7, pp. 3426–3437, Jul. 2016.

[9] Y. Yan, W. Ren, Y. Guo, R. Wang, and X. Cao, "Image deblurring via extreme channels prior," in *Proc. IEEE Conf. Comput. Vis. Pattern Recognit. (CVPR)*, Jul. 2017, pp. 4003–4011.

[10] D. Perrone and P. Favaro, "Total variation blind deconvolution: The devil is in the details," in *Proc. IEEE Conf. Comput. Vis. Pattern Recognit. (CVPR)*, Jun. 2014, pp. 2909–2916.

[11] W.-S. Lai, J.-J. Ding, Y.-Y. Lin, and Y.-Y. Chuang, "Blur kernel estimation using normalized color-line priors," in *Proc. IEEE Conf. Comput. Vis. Pattern Recognit. (CVPR)*, Jun. 2015, pp. 64–72.

[12] T. Michaeli and M. Irani, "Blind deblurring using internal patch recurrence," in *Proc. Eur. Conf. Comput. Vis. (ECCV)*, 2014, pp. 783–798.
[13] L. Xu, S. Zheng, and J. Jia, "Unnatural L0 sparse representation for natural image deblurring," in *Proc. IEEE Conf. Comput. Vis. Pattern Recognit. (CVPR)*, Jun. 2013, pp. 1107–1114.
[14] Y. Wang, J. Yang, W. Yin, and Y. Zhang, "A new alternating minimization algorithm for total variation image reconstruction," *SIAM J. Imag. Sci.*, vol. 1, no. 3, pp. 248–272, Aug. 2008.
[15] D. Krishnan and R. Fergus, "Fast image deconvolution using hyper-laplacian priors," in *Proc. Adv. Neural Inf. Process. Syst. (NIPS)*, 2009, pp. 1033–1041.
[16] D. Zoran and Y. Weiss, "From learning models of natural image patches to whole image restoration," in *Proc. IEEE Int. Conf. Comput. Vis. (ICCV)*, Nov. 2011, pp. 479–486.
[17] W. Dong, L. Zhang, G. Shi, and X. Li, "Nonlocally centralized sparse representation for image restoration," *IEEE Trans. Image Process.*, vol. 22, no. 4, pp. 1620–1630, Apr. 2013.
[18] J. Zhang, J. Pan, W.-S. Lai, R. Lau, and M.-H. Yang, "Learning fully convolutional networks for iterative non-blind deconvolution," in *Proc. IEEE Conf. Comput. Vis. Pattern Recognit. (CVPR)*, Jul. 2017, pp. 3817–3825.
[19] K. Zhang, W. Zuo, S. Gu, and L. Zhang, "Learning deep CNN denoiser prior for image restoration," in *Proc. IEEE Conf. Comput. Vis. Pattern Recognit. (CVPR)*, Jul. 2017, pp. 3929–3938.
[20] M. S. C. Almeida and M. A. T. Figueiredo, "Deconvolving images with unknown boundaries using the alternating direction method of multipliers," *IEEE Trans. Image Process.*, vol. 22, no. 8, pp. 3074–3086, Aug. 2013.
[21] W.-S. Lai, J.-B. Huang, Z. Hu, N. Ahuja, and M.-H. Yang, "A comparative study for single image blind deblurring," in *Proc. IEEE Conf. Comput. Vis. Pattern Recognit. (CVPR)*, Jun. 2016, pp. 1701–1709.
[22] U. Schmidt and S. Roth, "Shrinkage fields for effective image restoration," in *Proc. IEEE Conf. Comput. Vis. Pattern Recognit. (CVPR)*, Jun. 2014, pp. 2774–2781.
[23] D. Perrone, A. Ravichandran, R. Vidal, and P. Favaro, "Image priors for image deblurring with uncertain blur," in *Proc. Brit. Mach. Vis. Conf. (BMVC)*, 2012, pp. 1–11.
[24] Q. Shan, J. Jia, and A. Agarwala, "High-quality motion deblurring from a single image," *ACM Trans. Graph.*, vol. 27, no. 3, p. 73, 2008.
[25] L. Yuan, J. Sun, L. Quan, and H.-Y. Shum, "Progressive inter-scale and intra-scale non-blind image deconvolution," *ACM Trans. Graph.*, vol. 27, no. 3, p. 74, 2008.
[26] F. Heide, M. Rouf, M. B. Hullin, B. Labitzke, W. Heidrich, and A. Kolb, "High-quality computational imaging through simple lenses," *ACM Trans. Graph.*, vol. 32, no. 5, p. 149, Sep. 2013.
[27] H. Ji and K. Wang, "Robust image deblurring with an inaccurate blur kernel," *IEEE Trans. Image Process.*, vol. 21, no. 4, pp. 1624–1634, Apr. 2012.
[28] A. Goldstein and R. Fattal, "Blur-kernel estimation from spectral irregularities," in *Proc. Eur. Conf. Comput. Vis. (ECCV)*, 2012, pp. 622–635.
[29] S. Cho and S. Lee, "Fast motion deblurring," *ACM Trans. Graph.*, vol. 28, no. 5, p. 145, 2009.
[30] W. Hu, J. Xue, and N. Zheng, "PSF estimation via gradient domain correlation," *IEEE Trans. Image Process.*, vol. 21, no. 1, pp. 386–392, Jan. 2012.
[31] Z. Shen, "Wavelet frames and image restorations," in *Proc. Int. Congr. Math.*, 2010, pp. 1–29.
[32] S. Roth and M. J. Black, "Fields of experts," *Int. J. Comput. Vis.*, vol. 82, no. 2, pp. 205–229, Apr. 2009.
[33] A. Mosleh, J. M. P. Langlois, and P. Green, "Image deconvolution ringing artifact detection and removal via PSF frequency analysis," in *Proc. Eur. Conf. Comput. Vis. (ECCV)*, 2014, pp. 247–262.
[34] A. Chambolle, "An algorithm for total variation minimization and applications," *J. Math. Imag. Vis.*, vol. 20, nos. 1–2, pp. 89–97, 2004.
[35] K. Dabov, A. Foi, V. Katkovnik, and K. Egiazarian, "Image denoising with block-matching and 3D filtering," *Proc. SPIE*, vol. 6064A-30, p. 606414, Feb. 2006.
[36] S. Gu, L. Zhang, W. Zuo, and X. Feng, "Weighted nuclear norm minimization with application to image denoising," in *Proc. IEEE Conf. Comput. Vis. Pattern Recognit. (CVPR)*, Jun. 2014, pp. 2862–2869.
[37] U. Schmidt, C. Rother, S. Nowozin, J. Jancsary, and S. Roth, "Discriminative non-blind deblurring," in *Proc. IEEE Conf. Comput. Vis. Pattern Recognit. (CVPR)*, Jun. 2013, pp. 604–611.
[38] L. Bar, N. Kiryati, and N. Sochen, "Image deblurring in the presence of impulsive noise," *Int. J. Comput. Vis.*, vol. 70, no. 3, pp. 279–298, 2006.
[39] S. Cho, J. Wang, and S. Lee, "Handling outliers in non-blind image deconvolution," in *Proc. IEEE Int. Conf. Comput. Vis. (ICCV)*, Nov. 2011, pp. 495–502.
[40] R. Baraniuk, M. Davenport, R. DeVore, and M. Wakin, "A simple proof of the restricted isometry property for random matrices," *Constructive Approx.*, vol. 28, no. 3, pp. 253–263, Dec. 2008.
[41] E. J. Candès, "The restricted isometry property and its implications for compressed sensing," *Comp. Rendus Math.*, vol. 346, nos. 9–10, pp. 589–592, May 2008.
[42] C. Bishop, *Pattern Recognition and Machine Learning*. New York, NY, USA: Springer, 2006.
[43] L. Xu, Q. Yan, Y. Xia, and J. Jia, "Structure extraction from texture via relative total variation," *ACM Trans. Graph.*, vol. 31, no. 6, p. 139, Nov. 2012.
[44] L. Xu and J. Jia, "Two-phase kernel estimation for robust motion deblurring," in *Proc. Eur. Conf. Comput. Vis. (ECCV)*, 2010, pp. 157–170.
[45] L. Sun, S. Cho, J. Wang, and J. Hays, "Edge-based blur kernel estimation using patch priors," in *Proc. IEEE Int. Conf. Comput. Photogr. (ICCP)*, Apr. 2013, pp. 1–8.
[46] A. Beck and M. Teboulle, "A fast iterative shrinkage-thresholding algorithm for linear inverse problems," *SIAM J. Imag. Sci.*, vol. 2, no. 1, pp. 183–202, 2009.
[47] W. Zuo and Z. Lin, "A generalized accelerated proximal gradient approach for total-variation-based image restoration," *IEEE Trans. Image Process.*, vol. 20, no. 10, pp. 2748–2759, Oct. 2011.
[48] K. Schelten, S. Nowozin, J. Jancsary, C. Rother, and S. Roth, "Interleaved regression tree field cascades for blind image deconvolution," in *Proc. IEEE Winter Conf. Appl. Comput. Vis. (WACV)*, Jan. 2015, pp. 494–501.
[49] C. J. Schuler, M. Hirsch, S. Harmeling, and B. Schölkopf, "Learning to deblur," in *Proc. Workshop NIPS*, 2014, pp. 1–11.
[50] W. Zuo, D. Ren, D. Zhang, S. Gu, and L. Zhang, "Learning iteration-wise generalized shrinkage–thresholding operators for blind deconvolution," *IEEE Trans. Image Process.*, vol. 25, no. 4, pp. 1751–1764, Apr. 2016.
[51] Y. Chen, W. Yu, and T. Pock, "On learning optimized reaction diffusion processes for effective image restoration," in *Proc. IEEE Conf. Comput. Vis. Pattern Recognit. (CVPR)*, Jun. 2015, pp. 5261–5269.
[52] A. Levin, Y. Weiss, F. Durand, and W. T. Freeman, "Efficient marginal likelihood optimization in blind deconvolution," in *Proc. IEEE Conf. Comput. Vis. Pattern Recognit. (CVPR)*, Jun. 2011, pp. 2657–2664.
[53] R. Köhler, M. Hirsch, B. Mohler, B. Schölkopf, and S. Harmeling, "Recording and playback of camera shake: Benchmarking blind deconvolution with a real-world database," in *Proc. Eur. Conf. Comput. Vis. (ECCV)*, 2012, pp. 27–40.
[54] D. Martin, C. Fowlkes, D. Tal, and J. Malik, "A database of human segmented natural images and its application to evaluating segmentation algorithms and measuring ecological statistics," in *Proc. IEEE Int. Conf. Comput. Vis. (ICCV)*, Jul. 2001, pp. 416–423.

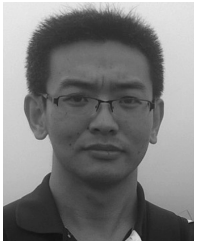

Dongwei Ren received the B.Sc. degree in bioinfomatics and the M.Sc. degree in computer science and technology from the Harbin Institute of Technology, Harbin, China, in 2011 and 2013, respectively. He is currently pursuing the joint Ph.D. degree with the School of Computer Science and Technology, Harbin Institute of Technology, and with the Department of Computing, The Hong Kong Polytechnic University. From 2012 to 2013 and from 2014 to 2014, he was a Research Assistant with the Department of Computing, The Hong Kong Polytechnic University. His research interests include low level vision and discriminative learning.

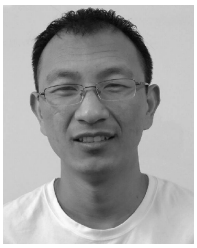

Wangmeng Zuo received the Ph.D. degree in computer application technology from the Harbin Institute of Technology, Harbin, China, in 2007. He is currently a Professor with the School of Computer Science and Technology, Harbin Institute of Technology. He has published over 60 papers in top-tier academic journals and conferences. His current research interests include image enhancement and restoration, object detection, visual tracking, and image classification. He has served as a Tutorial Organizer in ECCV 2016, an Associate Editor of the *IET Biometrics* and *Journal of Electronic Imaging*, and the Guest Editor of *Neurocomputing*, *Pattern Recognition*, IEEE TRANSACTIONS ON CIRCUITS AND SYSTEMS FOR VIDEO TECHNOLOGY, and IEEE TRANSACTIONS ON NEURAL NETWORKS AND LEARNING SYSTEMS.

David Zhang (F'08) received the degree in computer science from Peking University, the M.Sc. degree in 1982, and the Ph.D. degree in computer science from the Harbin Institute of Technology (HIT), in 1985, respectively. From 1986 to 1988, he was a Post-Doctoral Fellow with Tsinghua University and an Associate Professor with the Academia Sinica, Beijing. In 1994, he received the second Ph.D. degree in electrical and computer engineering from the University of Waterloo, Ontario, Canada. He is currently the Chair Professor with the Hong Kong Polytechnic University, since 2005, where he is the Founding Director of the Biometrics Research Centre (UGC/CRC) supported by the Hong Kong SAR Government in 1998. He is a Croucher Senior Research Fellow, Distinguished Speaker of the IEEE Computer Society, and a Fellow of IAPR. So far, he has published over 20 monographs, over 400 international journal papers and over 40 patents from USA/Japan/HK/China. He was selected as a Highly Cited Researcher in Engineering by Thomson Reuters in 2014, 2015, and 2016, respectively. He also serves as a Visiting Chair Professor with Tsinghua University and an Adjunct Professor with Peking University, Shanghai Jiao Tong University, HIT, and the University of Waterloo. He is Founder and Editor-in-Chief, International Journal of Image and Graphics, the Founder and the Series Editor, Springer International Series on Biometrics (KISB); Organizer, International Conference on Biometrics Authentication, an Associate Editor for over ten international journals including the IEEE Transactions and so on.

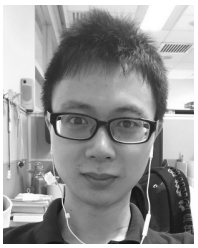

Jun Xu received the B.Sc. degree in pure mathematics and the M.Sc. degree in Information and Probability from the School of Mathematics Science, Nankai University, China, in 2011 and 2014, respectively. He is currently pursuing the Ph.D. degree with the Department of Computing, The Hong Kong Polytechnic University. His research interests include image restoration, subspace clustering, sparse, and low rank models.

Lei Zhang received the B.Sc. degree from the Shenyang Institute of Aeronautical Engineering, Shenyang, China, in 1995, and the M.Sc. and Ph.D. degrees in control theory and engineering from Northwestern Polytechnical University, Xian, China, in 1998 and 2001, respectively. From 2001 to 2002, he was a Research Associate with the Department of Computing, The Hong Kong Polytechnic University. From 2003 to 2006, he was a Postdoctoral Fellow with the Department of Electrical and Computer Engineering, McMaster University, Canada. In 2006, he joined as an Assistant Professor with the Department of Computing, The Hong Kong Polytechnic University, where he has been a Chair Professor, Since 2017. He has published over 200 papers in those areas. His research interests include computer vision, pattern recognition, image and video analysis, and biometrics. As of 2017, his publications have been cited over 28,000 times in the literature. He is an Associate Editor of the IEEE TRANSACTIONS ON IMAGE PROCESSING, *SIAM Journal of Imaging Sciences and Image and Vision Computing*. He is a Clarivate Analytics Highly Cited Researcher from 2015 to 2017.